Review Paper

Advances in thin film deposition at atmospheric pressure using dielectric barrier discharges

Fiorenza Fanelli[1]*, Piera Bosso[2], Anna Maria Mastrangelo[2], and Francesco Fracsssi[1,2]

[1]*National Research Council (CNR), Institute of Nanotechnology (NANOTEC) c/o Department of Chemistry, University of Bari Aldo Moro, via Orabona 4, 70126, Bari, Italy*

[2]*Department of Chemistry, University of Bari Aldo Moro, via Orabona 4, 70126, Bari, Italy*

E-mail: fiorenza.fanelli@cnr.it

Surface processing of materials by atmospheric pressure dielectric barrier discharges (DBDs) has experienced significant growth in recent years. Considerable research efforts have been directed for instance to develop a large variety of processes which exploit different DBD electrode geometries for the direct and remote deposition of thin films from precursors in gas, vapor and aerosol form. This article briefly reviews our recent progress in thin film deposition by DBDs with particular focus on process optimization. The following examples are provided: (i) the preparation of hybrid organic/inorganic nanocomposite coatings using an aerosol-assisted process, (ii) the plasma-enhanced chemical vapor deposition of thin films on a open-cell foam accomplished by igniting the DBD throughout the entire three-dimensional porous structure of the substrate, (iii) the DBD jet deposition of coatings containing carboxylic acid groups and the improvement of their chemical and morphological stability upon immersion in water.

1. Introduction

Among different atmospheric pressure cold plasmas, the dielectric barrier discharge (DBD) has attracted much interest in surface processing of materials due to its simple design, ease of generation, scalability to large area substrates.[1-5] In particular, in recent years, there have been considerable advances in the development of a large variety of processes which exploit the DBD for the direct and remote deposition of thin films from precursors in gas, vapor and aerosol form. [1-5]

Intense research efforts have been made to adapt the classical plasma-enhanced chemical vapor deposition (PECVD) processes to the specific features of DBD operation, as for instance the existence of different discharge regimes, the use of high flow rates of a dilution gas in combination with low concentrations of thin film precursors, the limitations imposed by the narrow gas gaps as well as the fluid dynamic issues associated to the feed mixture injection and discharge cell assembly.[1-2,6-20] On the other hand, innovative deposition strategies have been also developed, such as various aerosol-assisted processes[21-24] recently proposed for instance for the preparation of hybrid multicomponent coatings. [25-29]

It has been demonstrated that DBD-based processes can afford the preparation of a wide range of coatings, spanning from the high quality dense inorganic layers obtained by high current diffuse DBDs,[30] to the polymeric films characterized by superior retention of the monomer structure recently deposited using nanosecond pulsed DBDs.[31-32]

This paper proposes a short review of our recent advances in thin film deposition by DBDs; the examples described herein include:

(i) the PECVD of fluoropolymers on open-cell polyurethane foams,[33] reported to show the DBD potentiality for thin film deposition on the outer and inner surfaces of complex three-dimensional (3D) porous substrates;

(ii) the deposition of hydrocarbon polymer/ZnO nanoparticles nanocomposite (NC) thin films,[26,34] presented as an example of the preparation of multicomponent coatings by means of aerosol-assisted processes;

(iii) the DBD jet deposition of thin films containing carboxylic acid groups, reported to demonstrate the possibility of obtaining water-stable coatings functionalized with reactive moieties by DBD. [35]

For each of these examples, first, an overview of the existing literature is given, then details on DBD reactors and deposition conditions are provided with particular emphasis on process optimization, finally some representative results are presented.

2. PECVD of fluorocarbon coatings on open-cell foams

The low pressure PECVD has been successfully utilized for the surface modification of 3D porous materials, i.e., for the deposition of thin films onto their outer and inner surfaces, while leaving the bulk properties and porous architecture intact. [36-39)] Several studies on the treatment of polymeric scaffolds for tissue engineering applications enlightened that the diffusion of reactive depositing species into the scaffold interior controls thin film deposition in low pressure plasmas. It has been shown, in fact, that the limited penetration of thin film precursors within the 3D porous substrate generally results in gradients of the coating thickness and of the surface chemical composition moving from the exterior to the interior of the scaffold.[36-39)] The uniformity of the plasma treatment throughout the entire porous material could be improved if the discharge could ignite inside the pores of the substrate and, therefore, with atmospheric pressure operation. The possibility of igniting the DBD within porous structures on millimeter and submillimeter scales (e.g., ceramic foams and scaffolds) was already demonstrated,[40-42)] however contrary to expectations, this possibility has not been profitably exploited in materials processing so far. Therefore, we carried out an explorative study focused on the PECVD of fluorocarbon coatings onto the entire 3D network of open-cell foams (i.e. on their outer and inner surfaces), using a dielectric barrier discharge.[33)] To enlighten the potential of the DBD as a plasma inside complex porous materials, the following initial decisions were made regarding the substrate to be treated, the thin film to be deposited, the DBD reactor and deposition conditions to be used:

(i) We selected an open-cell foam substrate consisting of a 3D continuous network of interconnected solid struts, also referred to as ligaments. The isotropic fully open porous structure of the foam (no closed cells) allows the feed gas to flow and the DBD to ignite throughout the entire porous substrate during plasma treatments. Specifically, thin films were deposited on a commercial open-cell polyurethane (PU) foam characterized by porosity of about 97%, pore density of 30 pores per inch (ppi), minimum ligament width in the range 140-220 μm, pores dimension in the range 400-1300 μm. Rectangular foam strips, having a thickness of 5 mm, were used as substrates. [33)]

(ii) The fluorocarbon coating was deposited by a DBD fed with helium and hexafluoropropene (C_3F_6) at flow rates of 6000 sccm and 6 sccm, respectively. The choice of a fluoropolymer was motivated by the need to clearly distinguish the plasma-deposited coating from the underlying polyurethane substrate when the surface

composition of the plasma-treated foam was investigated by X-ray photoelectron spectroscopy (XPS). C_3F_6 was used as precursor because, as unsaturated fluorocarbon, it allows obtaining quite high polymerization rates both in low pressure[43] and atmospheric pressure plasmas[6].

(ii) Deposition processes were carried out using a DBD reactor with a parallel plate electrode configuration and lateral gas injection, described previously in full detail.[6,33] As shown in Fig. 1(a), during deposition processes the foam substrate was located in the center of the discharge region sandwiched between the dielectric-covered electrodes of the DBD system (i.e., both foam and gas gap have equal thickness of 5 mm), so that the feed mixture could be forced to flow through the interconnected porous structure of the foam. This allowed obtaining the ignition of the discharge both outside and inside the foam (Fig. 1(a)). The DBD was generated by applying a sinusoidal AC high voltage (20 kHz and 1.15 kV_{rms}) and operated in a filamentary regime.

Results from XPS analyses showed that, for a deposition time of 30 min, a good uniformity of the surface chemical composition is achieved over the entire substrate, i.e. on both the exterior and interior of the foam. In particular Fig. 1(b) and Fig. 1(c) report the high resolution C1s XPS spectra corresponding to the inner (i.e., foam cross-section obtained cutting the foam with a scalpel blade after plasma treatment) and outer surfaces of the plasma-treated foam (i.e., surfaces directly exposed to the discharge ignited in the ‘‘free’’ gas gap). Curve-fitting results show that the peak area percentages ascribed to CF, CF_2, and CF_3 groups are greater than 20%, the peak area percentage of the hydrocarbon component ascribable to the underlying polyurethane polymer remains below 4%, and the XPS F/C ratio (calculated from curve-fitting results) is about 1.4.[6,15,33] Interestingly, for a deposition time of 5min (i.e., the shorter deposition time used in our work), moderate changes in surface chemical composition moving from the outer to the inner surfaces of the plasma-treated foam were observed, since the interior of the foam presented a lower fluorination degree (F/C ratio of about 1.2) than the exterior (F/C ratios in the range 1.3-1.4). Comparative experiments carried out locating the foam substrate downstream of the discharge region, where the DBD does not ignite within the porous structure of the foam, showed considerably lower fluorination degrees into the foam interior, pointing out that in this case a very thin fluorocarbon layer was deposited.

Scanning electron microscopy (SEM) observations revealed that the porous architecture of the substrates was not modified by the plasma treatment (low-magnification image in Fig.

1(d)) and allowed estimating the thickness of the coating deposited on the struts of the foam for a deposition time of 30 min (Fig. 1(e)) . Considering the roughly triangular cross-section of the ligaments (indicated by the white arrow in Fig. 1(d)), the thickness of the coating seems to be greater on the vertices than on the sides of the ligaments (average thickness values of 440 ± 80 nn and 170 ± 30 nm for vertices and sides, respectively).[33] No appreciable variation of the coating average thickness was observed moving from the exterior to the interior surfaces of the foams.

3. Aerosol-assisted deposition of hydrocarbon polymer/ZnO nanoparticles nanocomposite coatings

The popularity of aerosol-assisted plasma deposition processes at atmospheric pressure has rapidly expanded over the last years.[21-29] One of the main motivations in utilizing these processes resides in the fact that they offer the unique possibility of injecting solutions or dispersions in the atmospheric plasma. This makes possible the deposition of hybrid multicomponent coatings in which for instance macromolecules (i.e., porphyrins, proteins, etc.)[27-29] or nanoparticles [25,26] are incorporated in a plasma-polymerized matrix.

Recently, we reported the deposition of organic-inorganic NC coatings by aerosol-assisted atmospheric cold plasma deposition.[26,34] The proposed method involves the utilization of a DBD fed with a carrier gas and the aerosol of a dispersion of preformed inorganic NPs in a liquid organic precursor. This allows the deposition, in a single step and under ambient conditions, of nanocomposite thin films consisting of NPs embedded to a certain extent in the organic component formed through plasma polymerization of the liquid precursor.

Specifically, in our work, hydrocarbon polymer/ZnO NPs NC coatings were prepared from dispersions of ZnO NPs in n-octane.[26] The DBD reactor used for thin films deposition is described in ref.[26] (Fig. 2(a)). The plasma is generated between two parallel plate electrodes both covered with an alumina plate, by applying a sinusoidal AC high voltage (22.0 ± 0.2 kHz, 2.6 ± 0.2 kV_{rms}) in pulsed mode (20 ms period, 13 ms plasma on-time, 65% duty cycle). During the deposition process the DBD is fed by helium (flow rate of 8000 sccm) and the aerosol of the dispersion generated by a pneumatic atomizer at a mass flow rate of 0.23 ± 0.02 g/min. Commercial ZnO nanoparticles with average particle size of 36 nm, nearly spherical shape and hexagonal crystal structure, were utilized. The surface of the NPs was first functionalized with oleate (capping) according to the procedure described elsewhere,[26] to obtain stable dispersions of polar ZnO NPs in nonpolar hydrocarbon solvents. It is worth

mentioning that crucial prerequisite for the utilization of this deposition strategy is, in fact, the good dispersibility of the NPs in a suitable solvent that also serves as precursor of the organic component of the NC layer.[25)]

Results from XPS and ATR-FTIR (attenuated total reflectance-Fourier transform infrared spectroscopy) analyses confirmed that the nanocomposite coatings present the chemical features of both the oleate-capped ZnO NPs and the polyethylene-like organic component originated from the plasma polymerization of n-octane. Additionally, SEM investigation showed that the NC thin film contains quasi-spherical agglomerates of ZnO nanoparticles (diameter ranging between 200 and 2200 nm) that lead to a hierarchical surface roughness; i.e., while the NPs agglomerates provide the micrometer-scale roughness, the NPs at the outer layer of the agglomerates provide the nano-roughness (Fig. 2(b))[26)]. The polyethylene-like polymer covers the NPs agglomerates to different extents and contributes to their immobilization in the three-dimensional network of the coating (Fig. 2(b)).

The chemical composition and morphology of the coatings can be varied over a wide range by changing the experimental parameters and, in particular, the composition of the starting dispersion. In fact, the increase of the NPs concentration in the starting dispersion promotes an increase of the ZnO content in the coating, allowing the surface roughness to become less influenced by the morphology of the polymer and more affected by the NPs agglomerates (cross-sectional SEM images in Fig. 2(c) and (d)). This ultimately leads to superhydrophobic surfaces with low contact angle hysteresis ((i.e., water contact angles greater than 150° and contact angle hysteresis less than 10°).[26)] Specifically, the superhydrophobic wetting properties of these coatings arise from the interplay of the hydrophobic character of the polymer and the surface roughness at micro- and nanoscales induced by NPs incorporation. In addition to superhydrophobicity, these plasma-deposited NC coatings exhibit also the peculiar photocatalytic properties of ZnO, as enlightened from our recent study of the photocatalytic degradation of a dye molecule (i.e., methylene blue) in water.[34)]

4. DBD jet deposition of thin films containing carboxylic acid groups

Thin films containing COOH groups have several applications; they can be used, for instance, to improve the adhesion of surfaces to polymers or inorganic materials, to enhance cell adhesion and growth, to increase the adsorption of basic species and

metals.[44-46] Therefore, the plasma deposition of this class of coatings has been widely investigated over the past two decades. Deposition processes are mostly performed using acrylic acid (AA) as thin film precursor. It has been shown that AA-fed plasmas both at low and atmospheric pressure easily allow the preparation of thin films characterized by high COOH groups concentrations,[19,21,45,47-52] that, in turn, are generally responsible of the poor water-stability of the layers.[45,47,48] However, for several applications such high COOH concentrations are very often not needed, instead good water-stability of the coatings is required. Therefore, one challenge in plasma deposition from acrylic acid is to obtain coatings with good chemical and morphological stability in water. It is worth mentioning that in low pressure plasmas this has been accomplished either by using high input power[45] or through plasma copolymerization (also referred to as codeposition) of AA and another monomer,[48,53,54] such as a unsaturated hydrocarbon that can act as crosslinker and/or chain-extender (e.g., 1,7-octadiene,[48] ethylene[54]).

We directed our efforts towards the preparation of water-stable coating containing COOH groups using a DBD fed with mixtures of AA and ethylene. The deposition was performed with a DBD jet to overcome one of the main drawbacks of the most diffuse DBDs geometries (e.g., parallel plate or coaxial cylindrical geometries), which, due to the narrow gas gap, impose limitation in the size and shape of substrates that can be processed.[4,55-58] However, it is worth mentioning that the optimization of deposition processes using plasma jets generally requires much effort, since many factors can affect the physical and chemical proprieties of the plasma plume. Moreover, in this specific case of study, to obtain water-stable coatings containing COOH groups using a DBD jet, we decided to act on the "input" chemistry of the deposition process (i.e., copolymerization of acrylic acid and ethylene), rather than on the electrical parameters of the discharge (e.g., increase of the input power to improve acrylic acid fragmentation and coating cross-linking). In fact, it is important to keep in mind that in the "remote" deposition by plasma jet, the action of the plasma on the growing polymer generally is much less effective and process control is often not straightforward, with respect to the "direct" deposition in which the substrate is located between the electrodes and the growing polymer is exposed directly to the action of the plasma and of active species formed near the substrate.

The deposition was performed using the plasma jet with coaxial cylindrical DBD configuration shown in Figure 3(a), described previously in detail.[35] The discharge was ignited at 20 kHz and 1.4 kV_{rms}, using 7 slm of He as main gas. The acrylic acid and ethylene concentrations in the feed were varied in the ranges 0-25 ppm and 0-360 ppm, respectively.

As assessed by XPS, in case of thin films deposited from helium/acrylic acid fed DBDs (no ethylene addition) the percentage of the XPS C1s component ascribed to carboxylic groups (i.e., both COOH and COOR moieties) can be increased from about 4% to 13% with increasing the acrylic acid concentration in the feed gas. However, after 72 h of water immersion, these films show significant reduction of the concentration of carboxylic groups, thickness loss up to 70% and considerable morphological changes.

Ethylene addition to AA mainly enhances the deposition rate (up to 29 nm/min), reduces the carboxylic groups content of the coatings, and significantly improves their chemical and morphological stability upon immersion in water. Fig. 3(b) shows the high resolution C1s XPS spectra of the coating obtained from acrylic acid/ethylene codeposition at the highest AA concentration used in our work ([AA] and [ethylene] of 25 and 200 ppm, respectively), before and after 72 h of soaking in water. In particular, a very slight decrease of percentage of carboxylic groups (i.e., COOH and COOR groups) can be observed after water immersion (from 9% to 8%). XPS analyses in conjunction with chemical derivatization with trifluoroethanol were carried out to unambiguously estimate the surface concentration of COOH groups; it was observed that the concentration of carboxylic acid groups remains almost constant upon water immersion (6.6 ± 0.6% and 6.1± 0.6% before and after 72 h water immersion, respectively). SEM analyses evidenced negligible morphological changes and low thickness loss (about 7%) after 72 h of water soaking (cross-sectional SEM images in Fig.3(d) and Fig. 3(e)).

4. Conclusions

In this short review we outlined our recent achievements in thin film deposition by DBDs, representing only a small part of the intense research efforts undertaken by the plasma chemistry community in this field.

We used a DBD fed with helium and hexafloropropene to deposit a fluorocarbon coating on a commercial PU foam. During plasma processes, the discharge was ignited both outside the foam and throughout its entire 3D porous structure, to allow the deposition of a fluoropolymer on both the outer and inner surfaces of the substrate. This study suggests new opportunities in surface processing of porous materials by DBDs. Future directions of this work include the investigation of different plasma conditions and feed mixtures, the use of foams characterized by higher pore density and, therefore, reduced pore dimension.

We investigated the deposition of hydrocarbon polymer/ZnO NPs NC coatings using an

aerosol-assisted process; hierarchical micro/nanostructured nanocomposite thin films containing quasi-spherical NPs agglomerates were obtained. Considering the versatility and generality of this deposition method, with particular regard to the possible combination of a wide range of NPs and organic precursors, this study provides a new direction to design and synthesize hierarchical organic-inorganic NC coatings. However, it is worth highlighting that this strategy is very different from the numerous low pressure plasma-based processes in which very often the formation of both the polymer matrix and the inorganic particles occurs in situ and in a single step. Also for this reason, the aerosol-assisted atmospheric plasma deposition is expected to lead, rather than to the replication of the same NC coatings successfully obtained with LP plasmas, to the enlargement of the range of structures and properties of organic-inorganic NCs deposited by cold plasma technologies.

Finally, we deposited water-stable coatings containing carboxylic acid groups utilizing a DBD plasma jet. Thin films deposited from acrylic acid/ethylene mixtures showed good chemical and morphological stability upon water immersion. As widely shown so far, the utilization of a plasma jet was intended to overcome the limitations imposed by the narrow gas gaps used in DBD electrode systems on the size and shape of substrates that can be processed.

Acknowledgments

The research was supported by the Italian Ministry for Education, University and Research (MIUR) under grants PONa3_00369, PON01_02239 and PON02_00576_3333604, and Regione Puglia under grant no. 51 “LIPP” within the Framework Programme Agreement APQ “Ricerca Scientifica”, II atto integrativo - Reti di Laboratori Pubblici di Ricerca. Danilo Benedetti, Savino Cosmai and Teresa Lasalandra are gratefully acknowledged for the skilful technical assistance.

References

1) F. Massines, C. Sarra-Bournet, F. Fanelli, N. Naude, and N. Gherardi, Plasma Process. Polym. **9**, 1041(2012).
2) F. Fanelli, Surf. Coat. Technol. **205**, 1536 (2010).
3) D. Pappas, J. Vac. Sci. Technol. A **29**, 020801 (2011).
4) T. Belmonte, G. Henrion, and T. Gries, J. Therm. Spray Technol. **20**, 744 (2011).
5) H. Kakiuchi, H. Ohmi, and K. Yasutake, J. Vac. Sci. Technol. A **32**, 030801 (2014).
6) F. Fanelli, G. Di Renzo, F. Fracassi, and R. d'Agostino, Plasma Process. Polym. **6**, S503, (2009).
7) F. Fanelli, F. Fracassi, and R. d'Agostino, Surf. Coat. Technol. **204**, 1779 (2010).
8) F. Fanelli, S. Lovascio, R. d'Agostino, and F. Fracassi, Plasma Process. Polym. **9**, 1132 (2012).
9) P. A. Premkumar, S. A. Starostin, H. de Vries, M. Creatore, P. M. Koenraad, W. A. MacDonald, and M. C. M. van de Sanden, Plasma Process. Polym. **9**, 1194 (2012).
10) O. Levasseur, L. Stafford, N. Gherardi, N. Naudé, V. Blanchard, P. Blanchet, B. Riedl, and A. Sarkissian, Plasma Process. Polym. **9**, 1168 (2012).
11) M. Kasuya, S. Yasui, and M. Noda, Jpn. J. Appl. Phys. **51**, 01AC01 (2012).
12) B. Nisol, G. Arnoult, T. Bieber, A. Kakaroglou, I. De Graeve, G. Van Assche, H. Terryn, and F. Reniers, Plasma Process. Polym. **11**, 335 (2014).
13) J. Vallade, R. Bazinett, L. Gaudy, and F. Massines, J. Phys D: Appl. Phys. **47**, 224006 (2014).
14) T. Witvrouwen, J. Dijkmans, S. Paulussen, and B. Sels, Plasma Process. Polym. **11**, 464 (2014).
15) J. Hubert, N. Vandencasteele, J. Mertens, P.l Viville,T. Dufour, C. Barroo, T. Visart de Bocarmé, R. Lazzaroni, and F. Reniers, Plasma Process. Polym. **12**, 1174 (2015).
16) J. Hubert, J. Mertens, T. Dufour, N. Vandencasteele, F. Reniers, P. Viville, R. Lazzaroni, M. Raes, and H. Terryn, J. Mater. Res. **30**, 3177 (2015).
17) T. Mori, Y. Futagami, E. Kishimoto, A. Shirakura, and T. Suzuki, J. Vac. Sci. Technol. A **33**, 060607 (2015).
18) S. Watson, B. Nisol, S. Lerouge, and M. R. Wertheimer, Langmuir **31**, 10125 (2015).
19) P. Cools. E. Sainz-García, N. De Geyter, A. Nikiforov, M. Blajan, K. Shimizu, F. Alba-Elías, C. Leys, and R. Morent, Plasma Process. Polym. **12**, 1153 (2015).
20) J. Philipp, A. K. Czerny, and C.-P. Klages, Plasma Process. Polym. (in press) [DOI: 10.1002/ppap.201500136].

21) L. J. Ward, W. C. E. Schofield, and J. P. S. Badyal, Chem. Mater. **15**, 1466 (2003).
22) P. Heyse, R. Dams, S. Paulussen, K. Houthoofd, Kris Janssen, P. A. Jacobs, and B. F. Sels, Plasma Process. Polym. **4**, 145 (2007).
23) J. Bardon, K. Apaydin, A Laachachi, M. Jimenez,T. Fouquet, F. Hilt, S. Bourbigot, and D. Ruch, Prog. Org. Coat. **88**, 39 (2015).
24) G. Mertz, T. Fouquet, H. Ibn El Ahrach, C. Becker, T. N. T. Phan, F. Ziarelli, D. Gigmes, and D. Ruch, Plasma Process. Polym. **12**, 1293 (2015).
25) F. Fanelli, and F. Fracassi, Plasma Chem. Plasma Process. **34**, 473 (2014).
26) F. Fanelli, A. M. Mastrangelo, and F. Fracassi, Langmuir **30**, 857 (2014) [Erratum **30**, 14111 (2014).
27) N. D. Boscher, D. Duday, P. Heier, K. Heinze, F. Hilt, and P. Choquet, Surf. Coat. Technol. **234**, 48 (2013).
28) G. Da Ponte, E. Sardella, F. Fanelli, S. Paulussen, and P. Favia, Plasma Process. Polym. **11**, 345 (2014).
29) F. Palumbo, G. Camporeale, Y.-W. Yang, J.-S. Wu, E. Sardella, G. Dilecce, C. D. Calvano, L. Quintieri, L. Caputo, F. Baruzzi, and P. Favia, Plasma Process. Polym. **12**, 1302 (2015).
30) S. A. Starostin, M. Creatore, J. B. Bouwstra, M. C. M. van de Sanden, and H. W. de Vries, Plasma Process. Polym. **12**, 545 (2015).
31) F. Hilt, Nicolas D. Boscher, David Duday, Nicolas Desbenoit, J. Levalois-Grutzmacher, and P. Choquet, ACS Appl. Mater. Interfaces **6**, 18418 (2014).
32) N. D. Boscher, F. Hilt, D. Duday, G. Frache, T. Fouquet, and P. Choquet, Plasma Process. Polym. **1**2, 66 (2015).
33) F. Fanelli, and F. Fracassi, Plasma Process. Polym. (in press) [DOI: 10.1002/ppap.201500150].
34) F. Fanelli, A. M. Mastrangelo, N. De Vietro, and F. Fracassi, Nanosci. Nanotechnol. Lett. **7**, 84 (2015).
35) P. Bosso, F. Fanelli, and F. Fracassi, Plasma Process. Polym. (in press) [DOI: 10.1002/ppap.201500005].
36) J. J. A. Barry, M. M. C. G. Silva, K. M. Shakesheff, S. M. Howdle, and M. R. Alexander, Adv. Funct. Mater. **15**, 1134 (2005).
37) F. Intranuovo, E. Sardella, R. Gristina, M. Nardulli, L. White, D. Howard, K. M. Shakesheff, M. R. Alexander, and P. Favia, Surf. Coat. Technol. **205**, S548 (2011).
38) F. Intranuovo, R. Gristina, F. Brun, S. Mohammadi, G. Ceccone, E. Sardella, F. Rossi, G.

Tromba, and P. Favia, Plasma Process. Polym. **11**, 184 (2014).

39) M. J. Hawker, A. Pegalajar-Jurado, and E. R. Fisher, Langmuir **30**, 12328 (2014).
40) M. Kraus, B Eliasson, U. Kogelschatz, and A. Wokaun, Phys. Chem. Chem. Phys. **3**, 294 (2001).
41) K. Hensel, V. Martisovits, Z. Machala, M. Janda, M. Lestinsky, P. Tardiveau, and A. Mizuno, Plasma Process. Polym. **4**, 682 (2007).
42) K. Hensel, Eur. Phys. J. D **54**, 141 (2009).
43) L. Sandrin, M. S. Silverstein, and E. Sacher, Polymer **42**, 3761 (2001).
44) V. Sciarratta, U. Vohrer, D. Hegemann, M. Muller, and C. Oehr, Surf. Coat. Technol. **174-175**, 805, (2003).
45) L. Detomaso, R. Gristina, G. S. Senesi, R. d'Agostino, and P. Favia, Biomaterials **26**, 3831 (2005).
46) N. De Vietro, R. d'Agostino, and F. Fracassi, Carbon **49**, 249 (2011).
47) R. Jafari, M. Tatoulian, W. Morscheidt, and F. Arefi-Khonsari, React. Funct. Polym. **66**, 1757 (2006).
48) M. R. Alexander, and T. M. Duc, Polymer **40**, 5479 (1999).
49) A. J. Beck, R. D. Short, and A. Matthews, Surf. Coat. Technol. **203**, 822 (2008).
50) O. Carton, D. B. Salem, S. Bhatt, J. Pulpytel, and F. Arefi-Khonsari, Plasma Process. Polym. **9**, 984 (2012).
51) R. Morent, N. De Geyter, M. Trentesaux, L. Gengembre, P. Dubruel, C. Leys, and E. Payen, Appl. Surf. Sci. **257**, 372 (2010).
52) M. Donegan, and D. P. Dowling, Surf. Coat. Technol. **234**, 53 (2013).
53) B. R. Pistillo, A. Perrotta, R. Gristina , G. Ceccone, M. Nardulli, R. d'Agostino, and Pietro Favia, Surf. Coat. Technol. **205**, S534 (2011).
54) D. B. Salem, O. Carton, H. Fakhouri, J. Pulpytel, and F. Arefi-Khonsari, Plasma Process. Polym. **11**, 269 (2014).
55) J. H. Yim, V. Rodriguez-Santiago, A.A. Williams, T Gougousi, D. D. Pappas, and J. K. Hirvonen, Surf. Coat. Technol. **234**, 21 (2013).
56) S. Bhatt, J. Pulpytel, S. Mori, M. Mirshahi, and F. Arefi-Khonsari, Plasma Process. Polym. **11**, 24 (2014).
57) S. Bhatt, J. Pulpytel, and F. Arefi-Khonsari, Surf. Innov. **3**, 63 (2015).
58) M. Bashir, and S. Bashir, Plasma Chem. Plasma Process. **35**, 739 (2015).

Figure Captions

Fig. 1. (Color online) (a) Schematic diagram showing the side view of the parallel plate DBD cell used for thin film deposition on PU foams positioned in the middle of the discharge region. High resolution C1s XPS spectra corresponding to the (b) inner (i.e., cross-section) and (c) outer surfaces of the plasma-treated foam. SEM images corresponding to the cross-section of the plasma-treated foam: (d) low magnification image, (e) image showing fine details of a cross-sectioned ligament where the deposited coating is clearly visible. Deposition time = 30 min.[33)]

Fig. 2. (Color online) (a) Schematic diagram of the DBD reactor used for the aerosol-assisted deposition of nanocomposite coatings. (b) SEM image of a typical quasi-spherical ZnO NPs agglomerate covered by a layer of hydrocarbon polymer. Cross-sectional SEM images of the NC coatings deposited from dispersions at different concentration of oleate-capped ZnO NPs in n-octane: (c) 0.5 and (c) and 5 wt %. Adapted from ref. [26)].

Fig. 3. (Color online) (a) Schematic diagram of the DBD jet used for the deposition of thin films containing carboxylic acid groups. High resolution C1s XPS spectra of coatings deposited from helium/acrylic acid/ethylene mixtures (b) before and (c) after 72 h of soaking in water. Cross-sectional SEM images of coatings deposited from helium/acrylic acid/ethylene mixtures (d) before and (e) after 72 h of soaking in water. [AA] = 25 ppm, [ethylene] = 200 ppm, deposition time = 10 min. [35)]

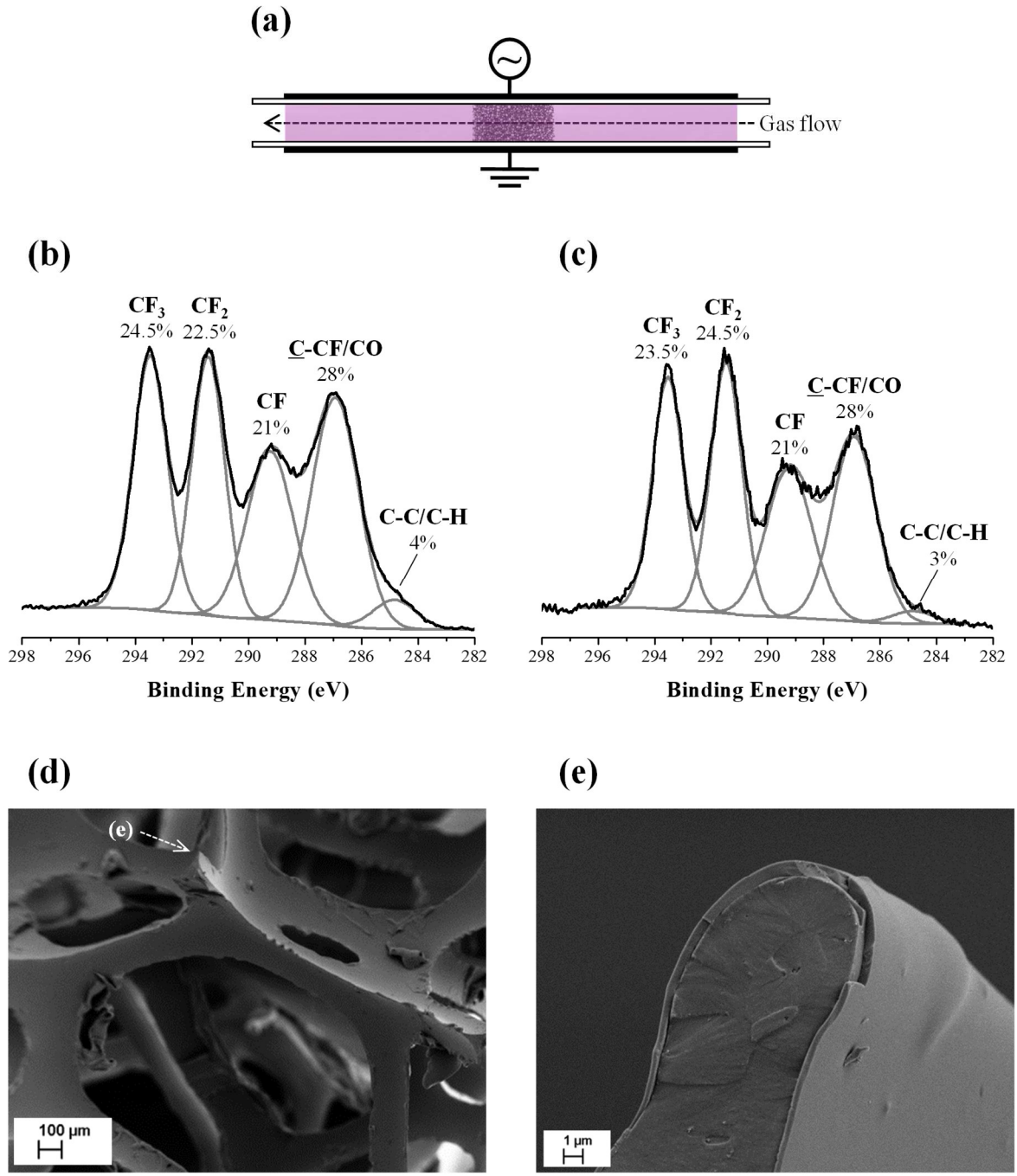

Fig.1. (Color Online)

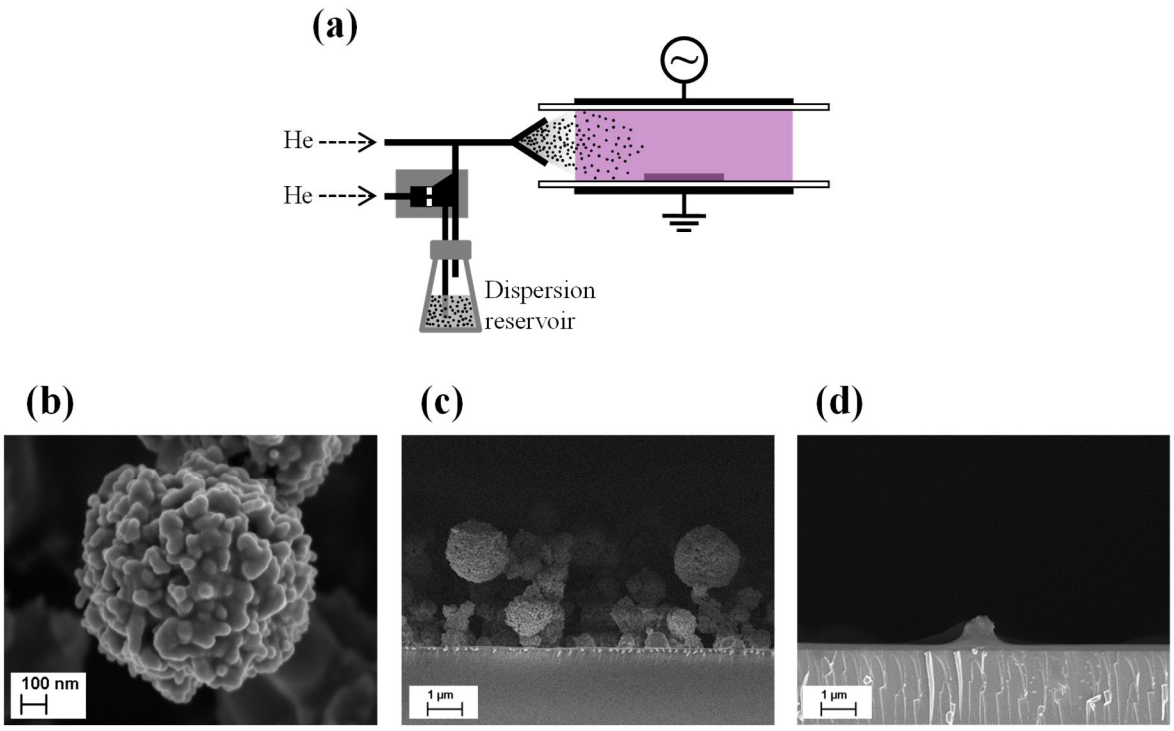

Fig.2. (Color Online)

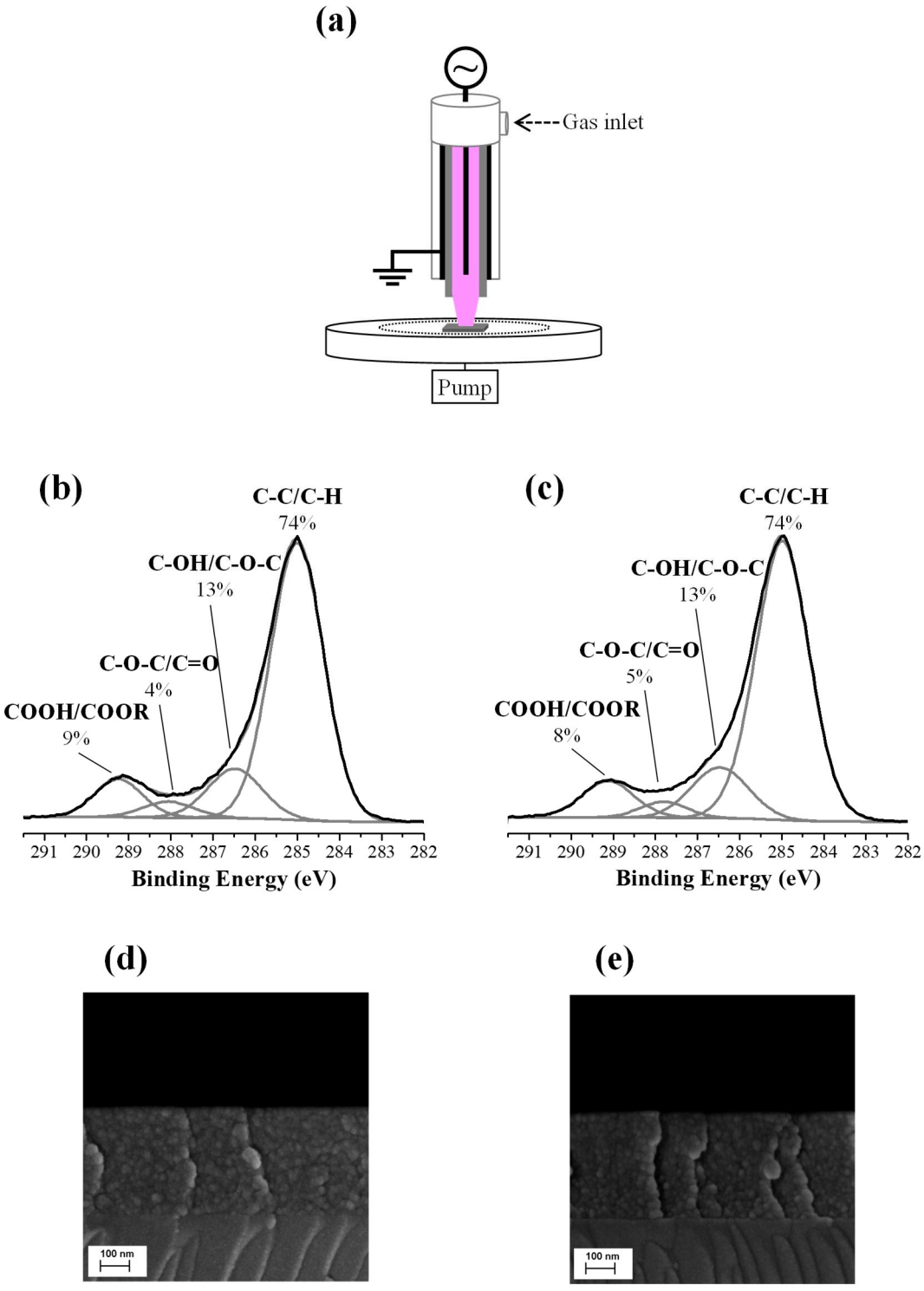

Fig.3. (Color Online)